Supporting Information

Ruthenium clusters decorating on lattice expanded hematite Fe_2O_3 for efficient electrocatalytic alkaline water splitting

Haibin Ma[a‡], Yongqiang Yang[b‡], Xiaohua Yu[c‡], Yang Zhao[d], Jiwei Ma[a*], Hongfei Cheng[a*]

a. *Shanghai Key Laboratory for R&D and Application of Metallic Functional Materials, Institute of New Energy for Vehicles, School of Materials Science and Engineering, Tongji University, Shanghai 201804, China.*

b. *Shenyang National Laboratory for Materials Science, Institute of Metal Research, Chinese Academy of Sciences, Shenyang 110016, China.*

c. *Faculty of Materials Science and Engineering, Kunming University of Science and Technology, Kunming 650093, China.*

d. *Dalian National Laboratory for Clean Energy (DNL), Dalian Institute of Chemical Physics, Chinese Academy of Science, Dalian 116023, China.*

‡These authors contributed equally to this work.

*Corresponding authors: cheng_hongfei@tongji.edu.cn; jiwei.ma@tongji.edu.cn

Methods

Synthesis of catalysts

In a typical procedure, 2 mol $FeCl_3$ and 1 mol NH_4Cl were homogeneously dispersed in 200 mL deionized water solution as the electrolyte. Then electrodeposition method was conducted using hydrophilic carbon cloth as the substrate at the constant current density of -1 mA cm^{-2} for 20 min to obtain Fe hydroxides nanosheets. The above Fe hydroxides nanosheets were annealed at 450 ^oC for 3 h under air atmosphere to obtain hematite Fe_2O_3 nanosheets. Lithiation process was operated in 7.5 mM LiOH aqueous electrolyte dissolving in deionized water by chronopotentiometry method using the self-supported hematite Fe_2O_3 electrode as the working electrode at constant current density of -0.5 mA cm^{-2} for 5 min. After lithiation, Ru clusters incorporation was realized by wet chemical impregnation method subsequently. In detail, the Li inserted hematite Fe_2O_3 was dispersed in homogeneous $RuCl_3$ aqueous solution with the concentration of 0.02 mM for 2 min and dried under vacuum condition for 12 h, thus our Ru/Fe_2O_3-Li catalyst was obtained.

Characterization

TEM, HAADF-STEM and EDS elemental mapping were performed on JEOL-JEM 2100F transmission electron microscope (with an accelerating voltage of 200 kV) equipped with an energy-dispersive detector. Spherical abbreviation corrected HR-TEM and HR-HAADF-STEM and corresponding EDS elemental mapping were performed on JEOL-JEM-ARM200F transmission electron microscope (operated on the HAADF mode with an accelerating voltage of 200 kV) equipped with an energy-dispersive detector. XPS data was obtained on an X-ray photoelectron spectrometer (Thermo ESCALab 250 Xi) with an excitation source of Al Kα radiation (hv = 1486.6 eV). XRD data was collected on a Bruker D8 Advance powder diffractometer (operating at 40 mA, 40 kV) equipped with a Cu-Kα source (λ_1 = 1.5405 Å, λ_2 = 1.5443 Å) and fitted with a beryllium window at room temperature. XAS measurements were conducted in the Shanghai Synchrotron Radiation Facility (SSRF). All the XAS

measurements were carried out at room temperature under ambient pressure. Data processing and EXAFS fitting were conducted using the Athena program.

Electrochemical measurements under a three-electrode system

In a typical test, the as-prepared self-supported electrodes served as the working electrode. All electrochemical measurements were conducted at room temperature in a typical three-electrode cell in 1.0 M aqueous KOH electrolyte. A carbon rod and a saturated calomel electrode (SCE) were used as the counter and reference electrodes, respectively. In this work, all potentials measured against SCE were converted to the reversible hydrogen electrode (RHE). The solution resistance was measured by potentiostatic electrochemical impedance spectroscopy at frequencies ranging from 0.1 Hz to 100 kHz. All measured potentials in electrochemical tests were 85% iR compensated unless otherwise specified. LSV curves were recorded with a scan rate of 10 mV/s. Before performance evaluation, all electrodes were electrochemically activated with CV scanning. Durability evaluation was examined by chronopotentiometry testing at constant current densities. EIS tests were performed at -0.02 V (versus RHE) from 0.1 Hz to 100 kHz. The ECSA was determined by the equation: ECSA = C_{dl}/C_s, where C_{dl} is the double-layer capacitance and C_s is the specific capacitance. In this study, a generally accepted C_s value of 0.035 mF cm^{-2} was adopted based on literatures.[1-2] C_{dl} was determined by the equation: $C_{dl} = i_c/\nu$, where i_c is half of the current difference between anode and cathode in the operating voltage window, ν is the scan rate. A series of CV curves in the non-Faradaic potential region 0.02-0.12 V (versus RHE) under different scan rates (5, 10, 15, 20, 25, 30 mV/s) were collected. By fitting different i_c values against the corresponding ν, C_{dl} was obtained from the slopes of linear fitting.

Alkaline electrolyzer test

For alkaline electrolyzer test, the as-fabricated self-supporting electrode Ru/Fe_2O_3-Li was used as both anode and cathode. For comparison, the commercial Pt/C (20wt% Pt

loading) and commercial RuO_2 were used as cathode and anode, respectively. Hydrophilic carbon cloth was used as the substrate for measurements. The loading amount of commercial Pt/C and commercial RuO_2 is 0.8 mg/cm^2. All the electrochemical curves were obtained at room temperature and ambient pressure. The stability was evaluated by chronopotentiometry method at current density of 10 mA cm^{-2} or 250 mA cm^{-2}.

Computational method

All calculations were performed by spin-polarized density functional theory (DFT) technique as applied in the Vienna Ab initio Simulation Package (VASP).[3-4] The Projector Augmented Wave (PAW) method and the Perdew-Burke-Ernzerhof (PBE) functional employing the Generalized Gradient Approximation (GGA) were adopted throughout the whole calculations.[5-8] All simulations were carried out using a 3 × 3 × 1 gamma-centered Monk horst Pack electronic k-point mesh with a 500 eV plane-wave cut-off energy.[9] A vacuum space of 20 Å was deployed along the z-direction to avoid mirror interactions between periodic images. The energy and force convergence criteria for each atom were chosen as 10^{-6} eV and 0.03 eV/Å, respectively.[10] The DFT-D3 method in the Grimme scheme was implemented to describe the van der Waals (vdW) interactions between reaction intermediates and catalysts.[11] VASP-sol incorporated implicit solvation was applied where the solvent parameters were those of water.[12] In addition, the relevant charge transfer caused by Li insertion and subsequently Ru cluster incorporation was quantitatively described by means of Bader charge analysis.[13-14]

The OER pathway was analyzed according to the electrochemical framework established by Nørskov et al.[15] In alkaline media, the OER processes would undergo the following four-electron steps:[16]

$$OH^- + {}^* \rightarrow OH^* + e^- \quad (1)$$

$$OH^* + OH^- \rightarrow O^* + H_2O + e^- \quad (2)$$

$$O^* + OH^- \rightarrow OOH^* + e^- \quad (3)$$

$$OOH^* + OH^- \rightarrow O_2 + H_2O + e^- \quad (4)$$

where * stands for the active site on the catalytic surface, OOH^*, O^*, and OH^* refer to the absorbed intermediates.

The equation to calculate the Gibbs free energy difference corresponding to OER pathway is as follows:[17]

$$\Delta G = \Delta E + \Delta E_{ZPE} - T\Delta S \quad (5)$$

where ΔE represents the energy difference between the reactant and product, calculated using DFT. ΔE_{ZPE} is the change in zero-point energy obtained by calculating the vibration frequency of the adsorbate. ΔS represents the change in entropy, with T set to room temperature (298.15 K).

All the calculations were performed by taking pH value of 0. The overpotential of OER is determined as follows:

$$\eta_{OER} = 1.23 - \Delta G_{min}/e \quad (6)$$

where ΔG_{min} is the minimum Gibbs free energy difference of the above four steps of OER, given by equation (1) minus equation (4); 1.23 V is the equilibrium potential of water for pH = 0 at temperature of 298.15 K.

The HER processes in alkaline media were generally accepted including the following two steps: water molecule dissociates into adsorbed H^* intermediate (Volmer step), then the produced H^* intermediate combines into H_2 molecule (either by Tafel step or Heyrovsky step depending on the HER kinetics):[18]

$$\text{Volmer step: } H_2O + e^- \rightarrow H^* + OH^-$$

$$\text{Tafel step: } H^* + H^* \rightarrow H_2$$

$$\text{Heyrovsky step: } H_2O + H^* + e^- \rightarrow H_2 + OH^-$$

And the overpotential of HER is determined as follows:

$$\eta_{HER} = \Delta G_{min}/e$$

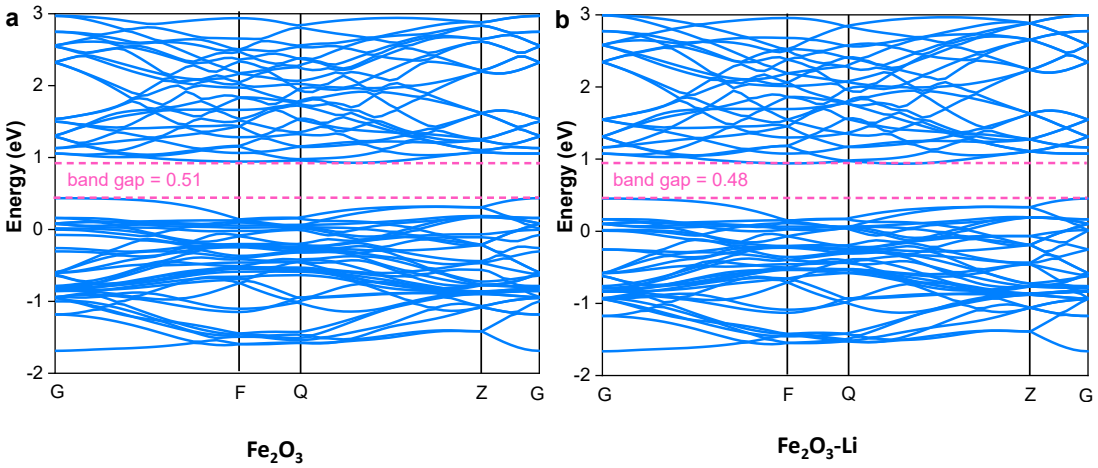

Figure S1. Calculated band structures of hematite Fe_2O_3 and Fe_2O_3-Li.

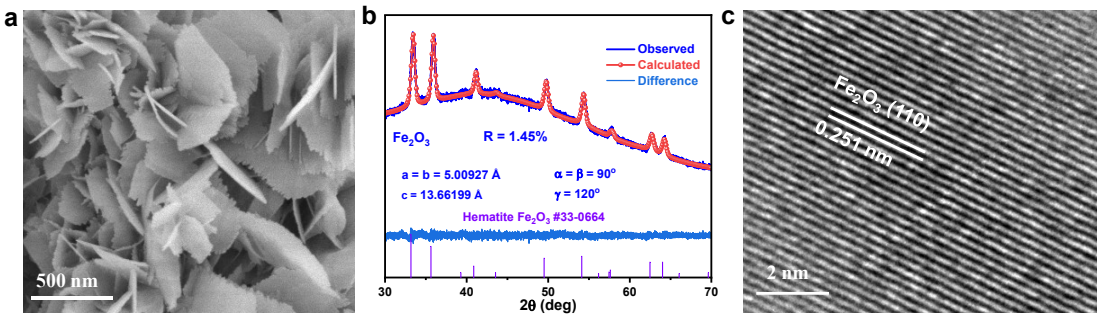

Figure S2. a) SEM image of hematite Fe_2O_3. b) Refined XRD pattern of hematite Fe_2O_3. c, HRTEM image of hematite Fe_2O_3.

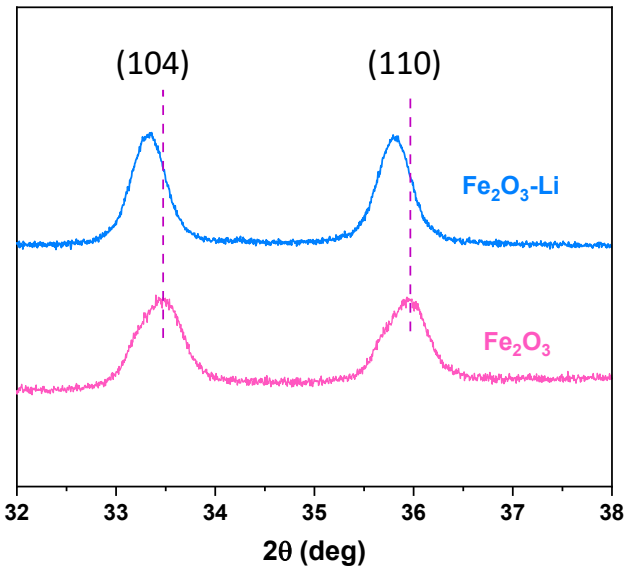

Figure S3. XRD pattern comparison for (104) and (110) facets of hematite Fe_2O_3 and Fe_2O_3-Li.

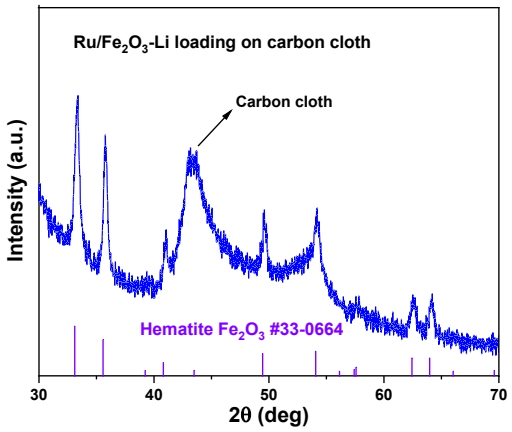

Figure S4. XRD pattern of Ru/Fe_2O_3-Li loading on carbon cloth, indicating no new crystal phases were formed after Ru clusters decoration.

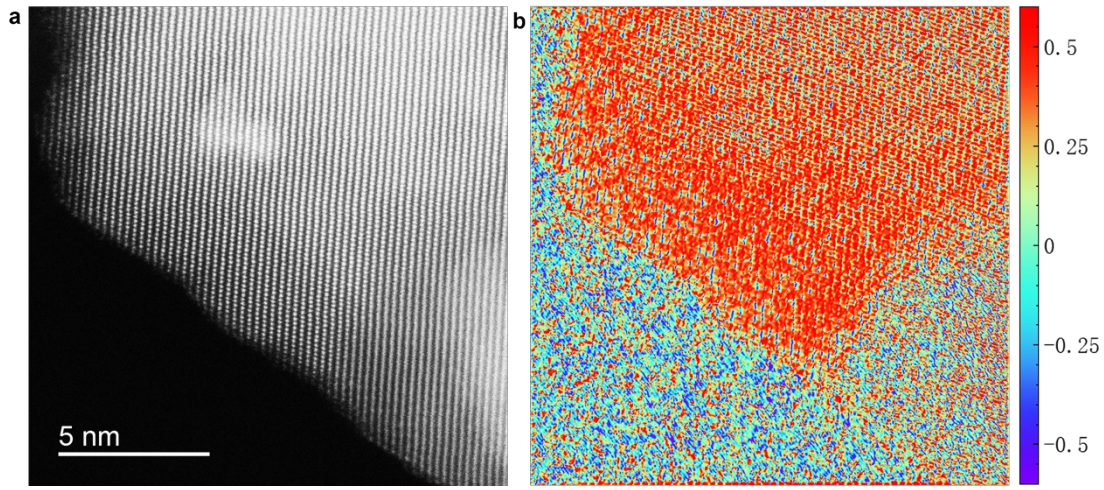

Figure S5. a) HAADF-STEM image of Ru/Fe_2O_3-Li. b) Corresponding simulated lattice distortion analysis of image a by GPA method.

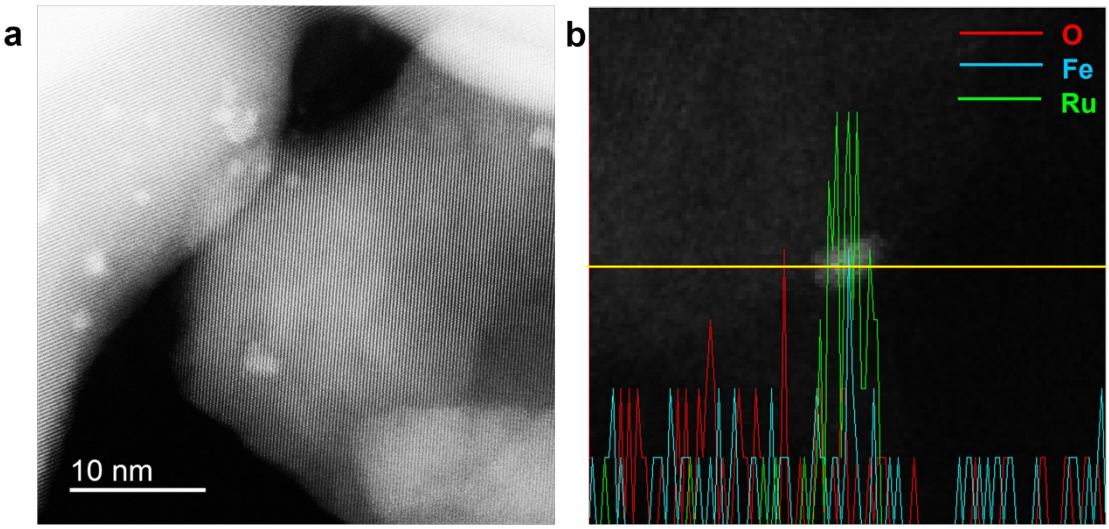

Figure S6. a) HAADF-STEM image of Ru/Fe_2O_3-Li. b) Line scan profile of Ru/Fe_2O_3-Li, obtained from the enlarged zone with one brightened particle in a).

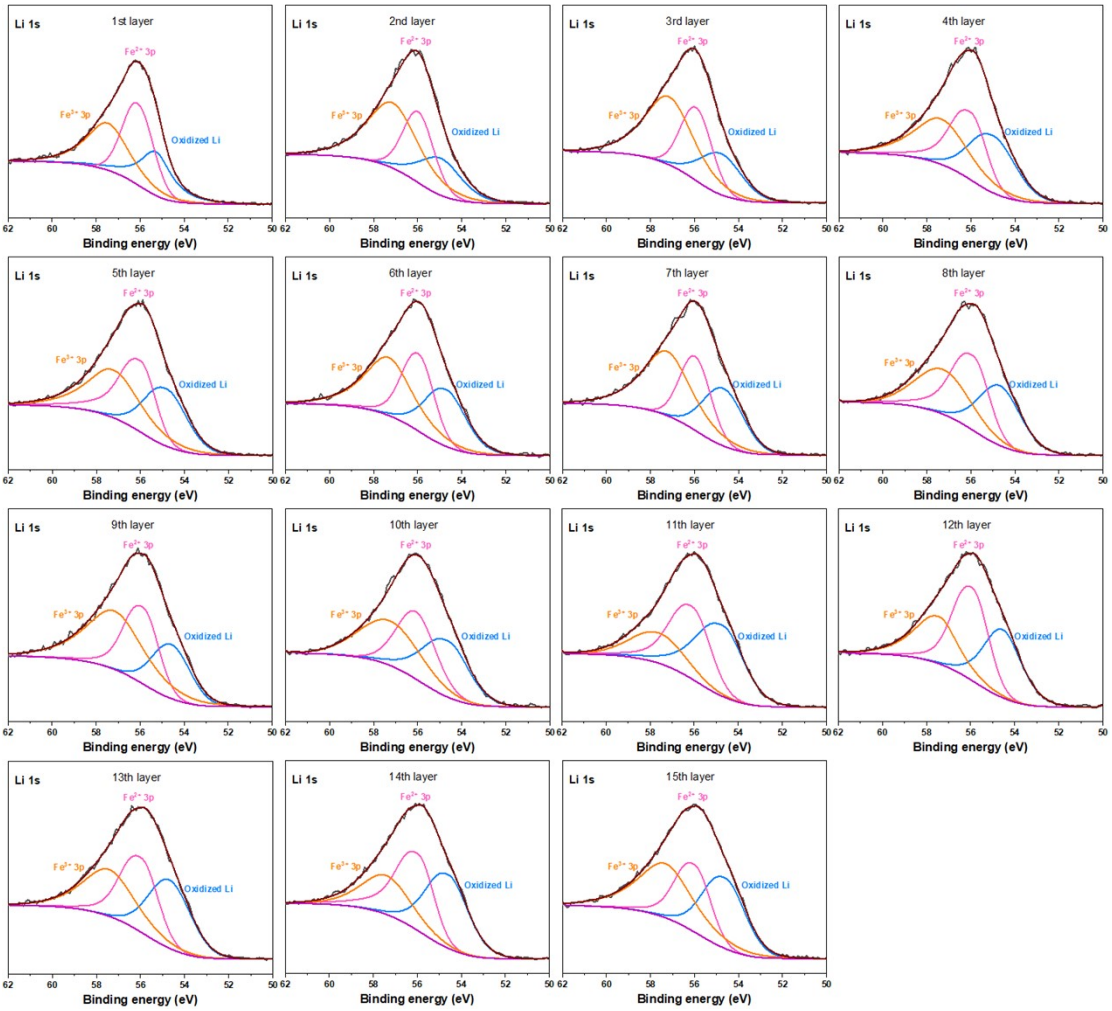

Atomic ratio of Li/Fe in high-resolution Li 1s spectra of Fe_2O_3-Li by XPS depth profiling

Etching times	Atomic ratio of Li/Fe
1st for 8 s (1st layer)	26.1/73.9
2nd for 8 s (2nd layer)	21.8/78.2
3rd for 8 s (3rd layer)	22.9/77.1
4th for 8 s (4th layer)	33.3/66.7
5th for 8 s (5th layer)	30.5/69.5
6th for 8 s (6th layer)	29.8/70.2
7th for 8 s (7th layer)	28.6/71.4
8th for 8 s (8th layer)	31.6/68.4
9th for 8 s (9th layer)	24.0/76.0

10th for 8 s (10th layer)	33.2/66.8
11th for 8 s (11th layer)	43.2/56.8
12th for 8 s (12th layer)	32.4/67.6
13th for 8 s (13th layer)	34.4/65.6
14th for 8 s (14th layer)	38.3/61.7
15th for 8 s (15th layer)	34.4/65.6

Generally, 1 s can etch 0.25-0.3 nm from surface.

Figure S7. Depth profiling analysis for high-resolution Li 1s XPS spectra of Fe_2O_3-Li, the corresponding atomic ratios of Li/Fe are listed in the table below.

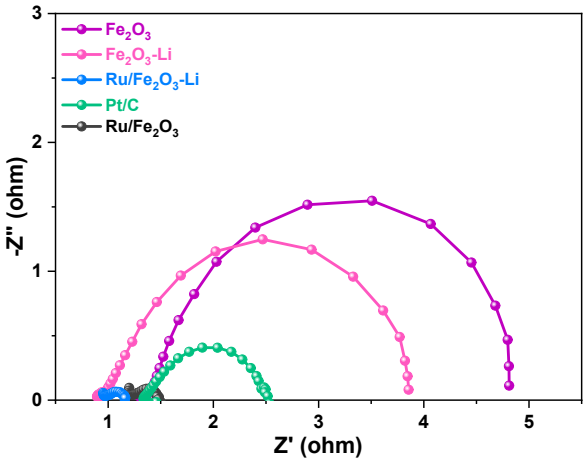

Figure S8. EIS spectra of Fe_2O_3, Fe_2O_3-Li, Ru/Fe_2O_3, Ru/Fe_2O_3-Li and commercial Pt/C catalysts under the potential of -0.02 V vs. RHE.

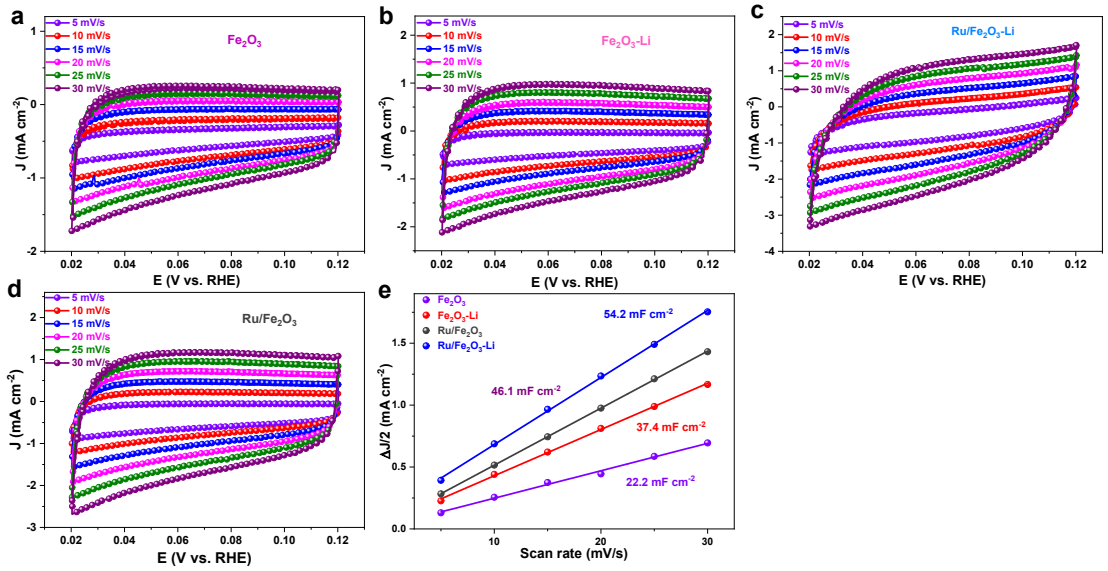

Figure S9. The CV curves of a, Fe_2O_3; b, Fe_2O_3-Li; c, Ru/Fe_2O_3-Li; d, Ru/Fe_2O_3 catalysts under non-Faradaic region at different scan rates and e the corresponding linear fitting for C_{edl} measurements.

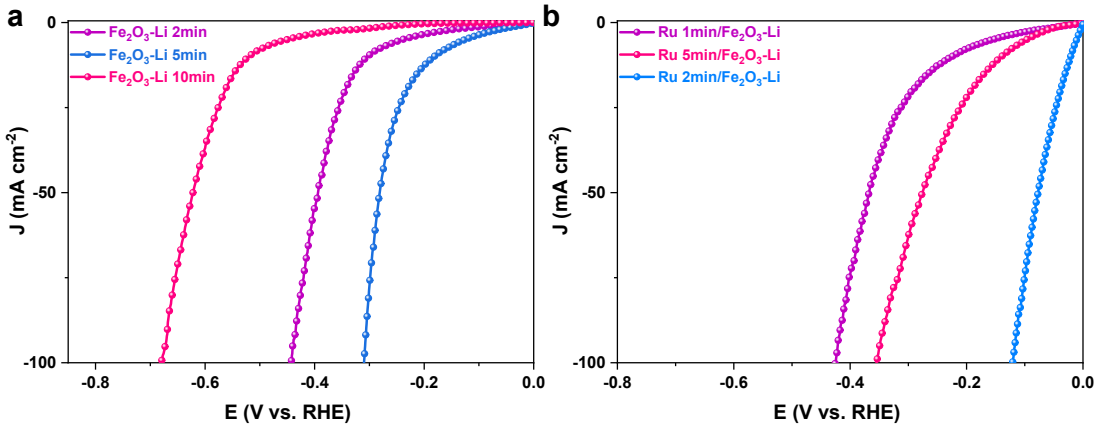

Figure S10. The influence of a) Li and b) Ru loading amount on the alkaline HER activity of Fe_2O_3. The catalysts are denoted based on the synthesis procedure. Detailly, Fe_2O_3-Li 2min: lithiation at -0.5 mA cm^{-2} for 2 min; Fe_2O_3-Li 5min: lithiation at -0.5 mA cm^{-2} for 5 min; Fe_2O_3-Li 10min: lithiation at -0.5 mA cm^{-2} for 10 min. Ru 1min/Fe_2O_3-Li: lithiation at -0.5 mA cm^{-2} for 5 min, and wet impregnation in 0.02 mM $RuCl_3$ for 1 min; Ru 2min/Fe_2O_3-Li: lithiation at -0.5 mA cm^{-2} for 5 min, and wet impregnation in 0.02 mM $RuCl_3$ for 2 min; Ru 5min/Fe_2O_3-Li: lithiation at -0.5 mA cm^{-2} for 5 min, and wet impregnation in 0.02 mM $RuCl_3$ for 5 min.

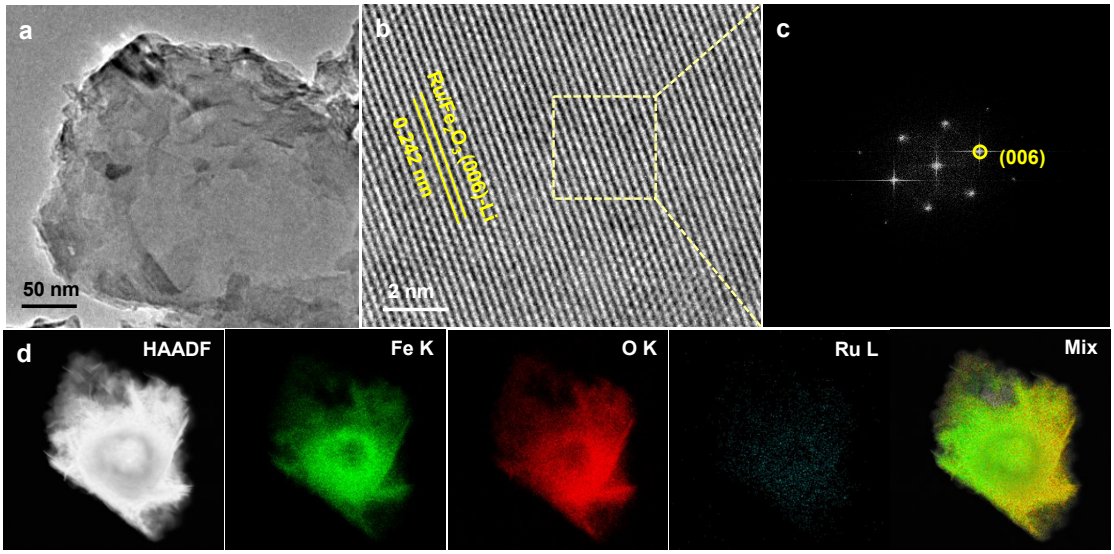

Figure S11. a) TEM, b) HRTEM, and c) SAED pattern images of Ru/Fe_2O_3-Li catalysts after alkaline HER stability measurement. d) EDS mapping images of Ru/Fe_2O_3-Li catalyst after HER stability test, green for Fe-K, red for O-K, blue for Ru-L and the corresponding mixture of above three elements.

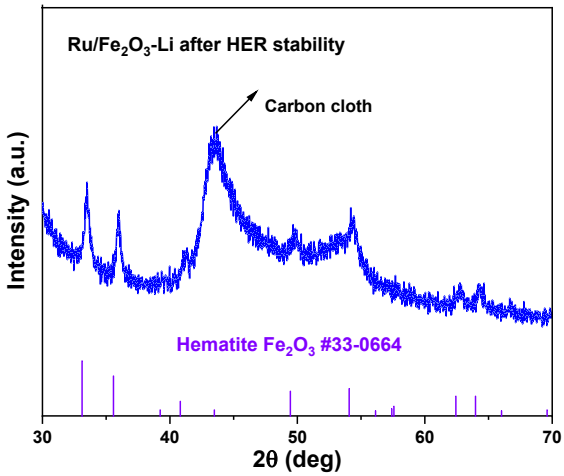

Figure S12. The XRD pattern of Ru/Fe_2O_3-Li catalyst after alkaline HER stability test.

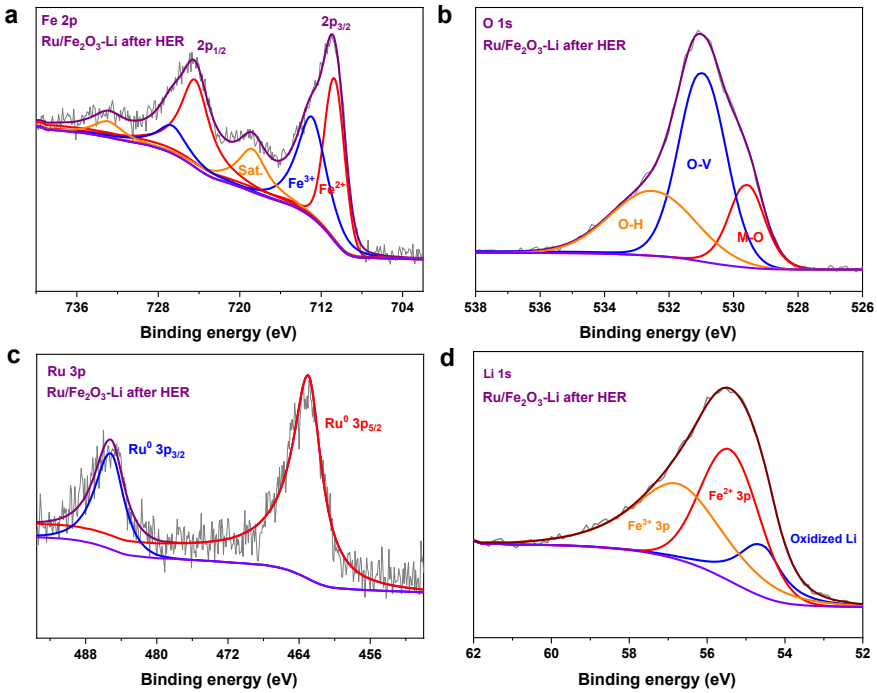

Figure S13. High-resolution XPS spectra of Ru/Fe_2O_3-Li after alkaline HER stability test. a) Fe 2p; b) O 1s; c) Ru 3p; d) Li 1s.

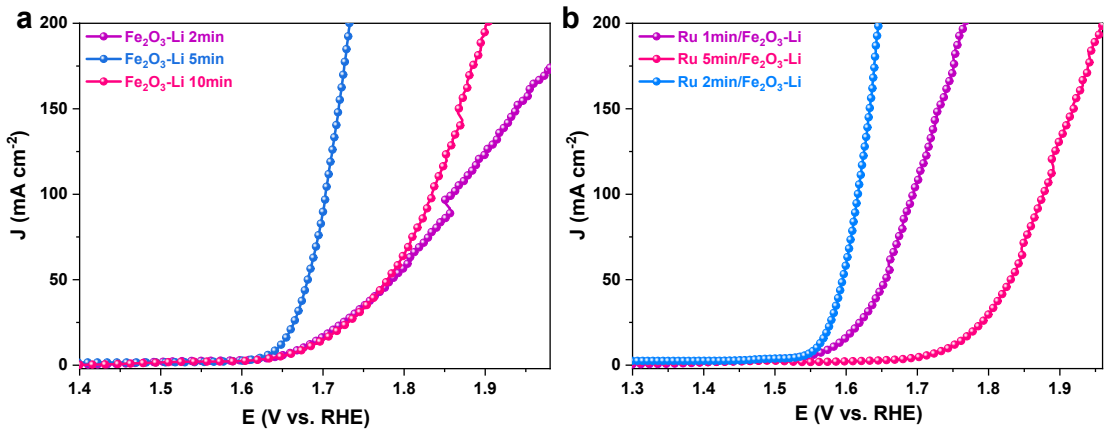

Figure S14. The influence of a) Li and b) Ru loading amount on the alkaline OER activity. The catalysts are denoted based on the synthesis procedure. Detailly, Fe_2O_3-Li 2min: lithiation at -0.5 mA cm^{-2} for 2 min; Fe_2O_3-Li 5min: lithiation at -0.5 mA cm^{-2} for 5 min; Fe_2O_3-Li 10min: lithiation at -0.5 mA cm^{-2} for 10 min. Ru 1min/Fe_2O_3-Li: lithiation at -0.5 mA cm^{-2} for 5 min, and wet impregnation in 0.02 mM $RuCl_3$ for 1 min; Ru 2min/Fe_2O_3-Li: lithiation at -0.5 mA cm^{-2} for 5 min, and wet impregnation in 0.02 mM $RuCl_3$ for 2 min; Ru 5min/Fe_2O_3-Li: lithiation at -0.5 mA cm^{-2} for 5 min, and wet impregnation in 0.02 mM $RuCl_3$ for 5 min.

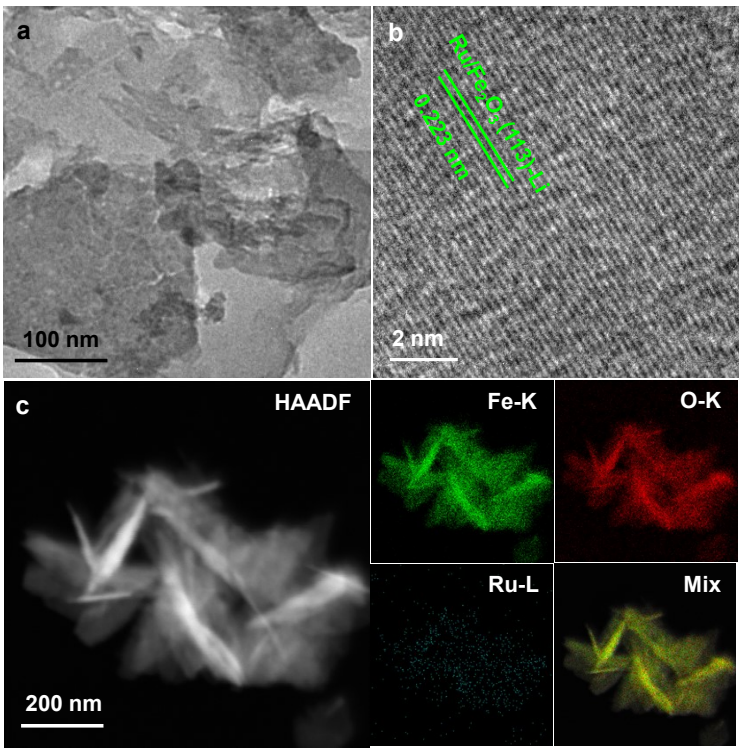

Figure S15. a) TEM, and b) HRTEM images of Ru/Fe_2O_3-Li after alkaline OER stability test. c) STEM image and the corresponding EDS mapping images of Ru/Fe_2O_3-Li after OER stability test.

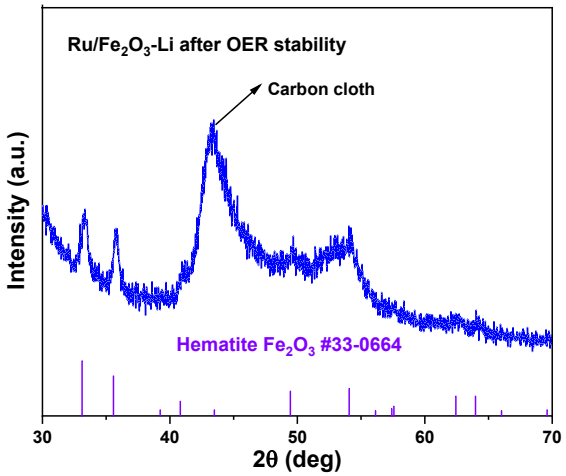

Figure S16. The XRD pattern of Ru/Fe_2O_3-Li catalyst after alkaline OER stability test.

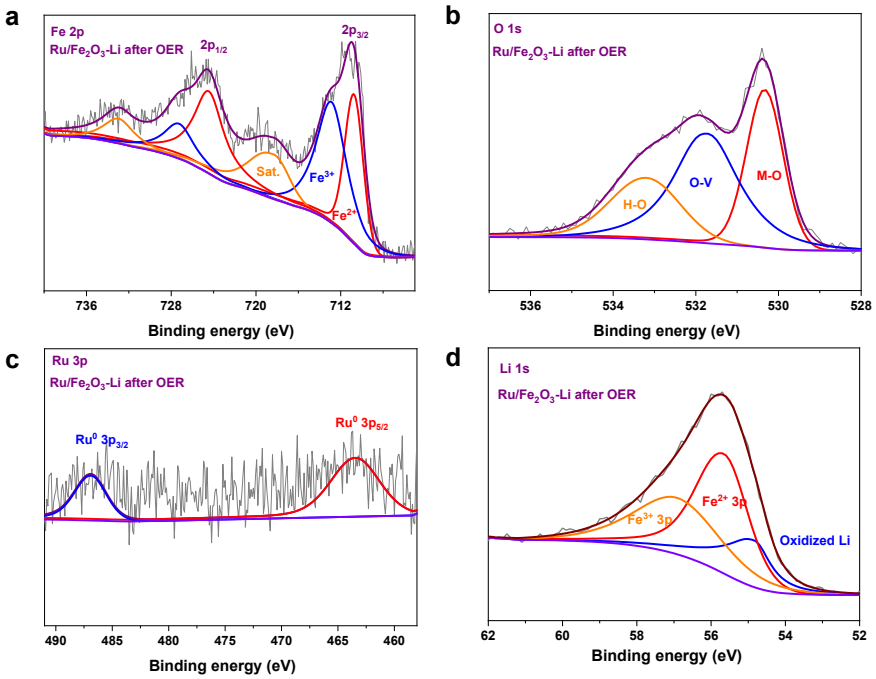

Figure S17. High-resolution XPS spectra of Ru/Fe_2O_3-Li after alkaline OER stability test: a) Fe 2p, b) O 1s, c) Ru 3p, and d) Li 1s.

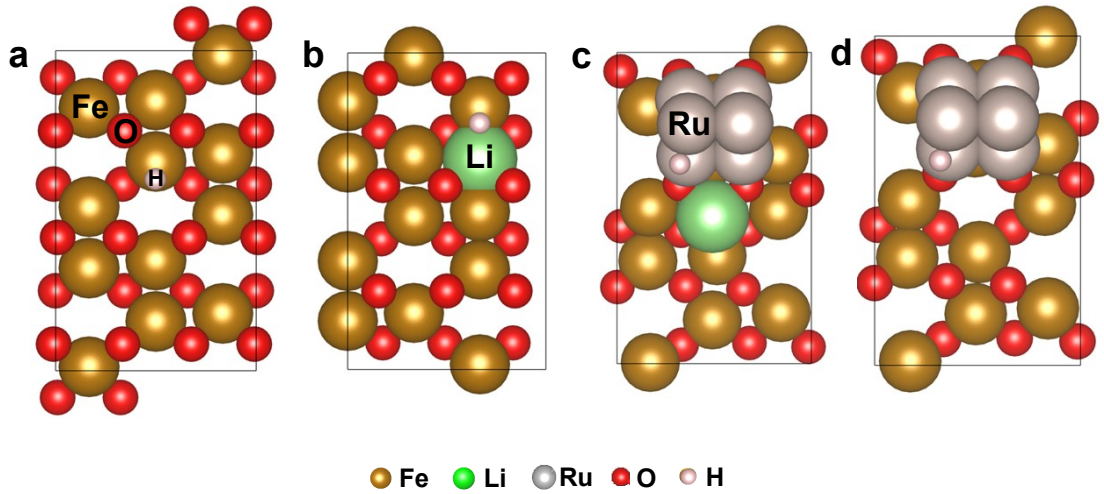

Figure S18. DFT-tested optimal sites for H^* adsorption on a) Fe_2O_3, b) Fe_2O_3-Li, c) Ru/Fe_2O_3-Li, and d) Ru/Fe_2O_3.

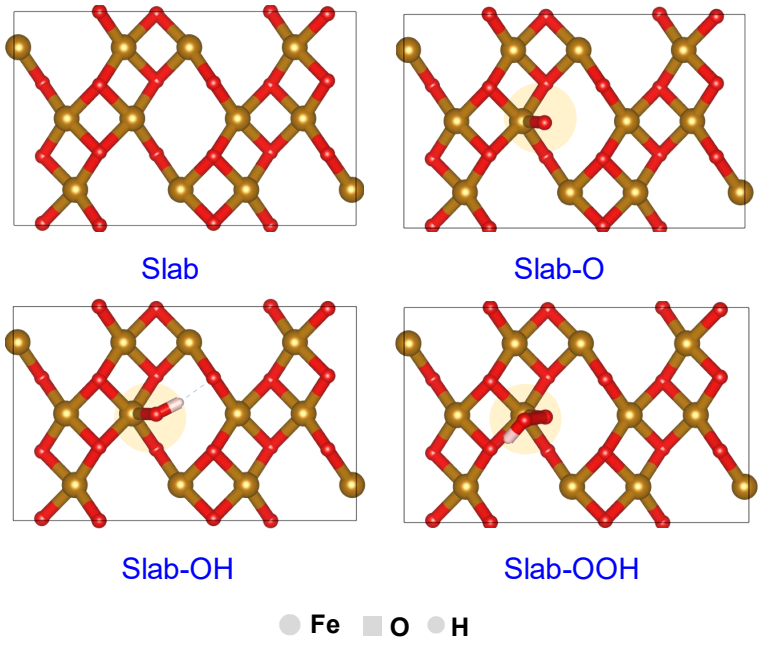

Figure S19. The DFT-tested optimal active site on hematite Fe_2O_3 (110) for $^*O$, $^*OH$, and $^*OOH$ adsorption.

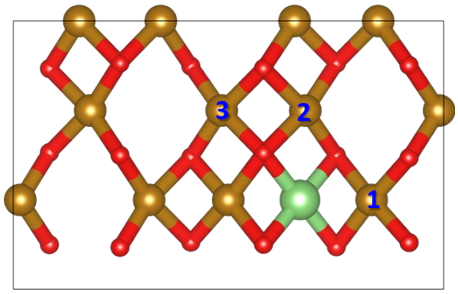

1	The tested OER pathway on Fe_2O_3 (110)-Li in acidic media								In alkaline media pH=14		
									4*0.0592pH		
	E (DFT) / eV	Δ*G* / eV	G / eV			0 V	1.23 V	Overpotential	0 V	0.401 V	Overpotential
Slab-1	-217.2367638	0	-217.2367638	$+2H_2O$	-245.6767638	0	0	0	0	0	0
OH	-227.0691164	0.315209	-226.7539074	$+H_2O+1/2\ H_2$	-244.3739074	1.30285638	0.072856	0.072856	0.473856	0.072856	0.07285638
O	-222.1272352	0.051558	-222.0756772	$+H_2O+H_2$	-243.0956772	2.58108663	0.121087	**0.04823**	0.923087	0.121087	**0.04823025**
OOH	-231.2750855	0.336005	-230.9390805	$+3/2\ H_2$	-241.1390805	4.53768334	0.847683	**0.726597**	2.051683	0.848683	0.72759671
Slab-2	-217.2367638	0	-217.2367638	$+O_2+2H_2$	-240.7467638	4.93	0.01	-0.83768	1.615	0.011	-0.83768334
O_2	-289.963	0.058	-289.905	O_2	-289.905						

2	The tested OER pathway on Fe_2O_3 (110)-Li in acidic media								In alkaline media pH=14		
									4*0.0592pH		
	E (DFT) / eV	Δ*G* / eV	G / eV			0 V	1.23 V	Overpotential	0 V	0.401 V	Overpotential
Slab-1	-217.2367638	0	-217.2367638	$+2H_2O$	-245.6767638	0	0	0	0	0	0
OH	-226.9156755	0.315209	-226.6004665	$+H_2O+1/2\ H_2$	-244.2204665	1.45629731	0.226297	0.226297	0.627297	0.226297	0.22629731
O	-222.1	0.051558	-222.048442	$+H_2O+H_2$	-243.068442	2.6083218	0.148322	**-0.07798**	0.950322	0.148322	**-0.07797551**
OOH	-231.1	0.336005	-230.763995	$+3/2\ H_2$	-240.963995	4.7127688	1.022769	**0.874447**	2.226769	1.023769	0.875447
Slab-2	-217.2367638	0	-217.2367638	$+O_2+2H_2$	-240.7467638	4.93	0.01	-1.01277	1.615	0.011	-1.0127688
O_2	-289.963	0.058	-289.905	O_2	-289.905						

3	The tested OER pathway on Fe_2O_3 (110)-Li in acidic media								In alkaline media pH=14		
									4*0.0592pH		
	E (DFT) / eV	Δ*G* / eV	G / eV			0 V	1.23 V	Overpotential	0 V	0.401 V	Overpotential
Slab-1	-217.2367638	0	-217.2367638	$+2H_2O$	-245.6767638	0	0	0	0	0	0
OH	-226.957431	0.315209	-226.642222	$+H_2O+1/2\ H_2$	-244.262222	1.41454176	0.184542	0.184542	0.585542	0.184542	0.18454176
O	-222.1290108	0.051558	-222.0774528	$+H_2O+H_2$	-243.0974528	2.57931096	0.119311	**-0.06523**	0.921311	0.119311	**-0.0652308**
OOH	-231.5869817	0.336005	-231.2509767	$+3/2\ H_2$	-241.4509767	4.22578708	0.535787	**0.416476**	1.739787	0.536787	0.41747612
Slab-2	-217.2367638	0	-217.2367638	$+O_2+2H_2$	-240.7467638	4.93	0.01	-0.52579	1.615	0.011	-0.52578708
O_2	-289.963	0.058	-289.905	O_2	-289.905						

Figure S20. The DFT-testing process for finding optimal active site of alkaline OER on Fe_2O_3 (110)-Li, suggesting site 3 is the optimal active site.

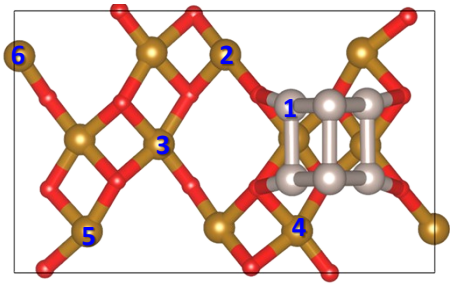

Fe Ru O

1 The tested OER pathway on Ru/Fe_2O_3 (110) in acidic media — In alkaline media pH = 14

4*0.0592pH

	E (DFT) / eV	Δ*G* / eV	G / eV			0 V	1.23 V	Overpotential	0 V	0.401 V	Overpotential
Slab-1	-257.1019347	0	-257.1019347	$+2H_2O$	-285.5419347	0	0	0	0	0	0
OH	-269.8942792	0.274	-269.6202792	$+H_2O+1/2\ H_2$	-287.2402792	-1.69834449	-2.92834	-2.92834	-2.52734	-2.92834	-2.92834449
O	-265.0304475	0.025	-265.0054475	$+H_2O+H_2$	-286.0254475	-0.48351281	-2.94351	**-0.01517**	-2.14151	-2.94351	**-0.01516832**
OOH	-273.273848	0.334	-272.939848	$+3/2\ H_2$	-283.139848	2.40208669	-1.28791	1.6556	-0.08391	-1.28691	1.6565995
Slab-2	-257.1019347	0	-257.1019347	$+O_2+2H_2$	-280.6119347	4.93	0.01	1.297913	1.615	0.011	1.29791331
O_2	-289.963	0.058	-289.905	O_2	-289.905						

2 The tested OER pathway on Ru/Fe_2O_3 (110) in acidic media — In alkaline media pH = 14

4*0.0592pH

	E (DFT) / eV	Δ*G* / eV	G / eV			0 V	1.23 V	Overpotential	0 V	0.401 V	Overpotential
Slab-1	-257.1019347	0	-257.1019347	$+2H_2O$	-285.5419347	0	0	0	0	0	0
OH	-267.7866683	0.274	-267.5126683	$+H_2O+1/2\ H_2$	-285.1326683	0.40926636	-0.82073	-0.82073	-0.41973	-0.82073	-0.82073364
O	-263.531298	0.025	-263.506298	$+H_2O+H_2$	-284.526298	1.01563665	-1.44436	**-0.62363**	-0.64236	-1.44436	**-0.62362971**
OOH	-273.273848	0.334	-272.939848	$+3/2\ H_2$	-283.139848	2.40208669	-1.28791	0.15645	-0.08391	-1.28691	0.15745004
Slab-2	-257.1019347	0	-257.1019347	$+O_2+2H_2$	-280.6119347	4.93	0.01	1.297913	1.615	0.011	1.29791331
O_2	-289.963	0.058	-289.905	O_2	-289.905						

3 The tested OER pathway on Ru/Fe_2O_3 (110) in acidic media — In alkaline media pH = 14

4*0.0592pH

	E (DFT) / eV	Δ*G* / eV	G / eV			0 V	1.23 V	Overpotential	0 V	0.401 V	Overpotential
Slab-1	-257.1019347	0	-257.1019347	$+2H_2O$	-285.5419347	0	0	0	0	0	0
OH	-268.2732237	0.274	-267.9992237	$+H_2O+1/2\ H_2$	-285.6192237	-0.07728903	-1.30729	-1.30729	-0.90629	-1.30729	-1.30728903
O	-261.556966	0.025	-261.531966	$+H_2O+H_2$	-282.551966	2.98996867	0.529969	1.837258	1.331969	0.529969	**1.8372577**
OOH	-273.2675738	0.334	-272.9335738	$+3/2\ H_2$	-283.1335738	2.40836088	-1.28164	-1.81161	-0.07764	-1.28064	-1.81060779
Slab-2	-257.1019347	0	-257.1019347	$+O_2+2H_2$	-280.6119347	4.93	0.01	1.291639	1.615	0.011	1.29163912
O_2	-289.963	0.058	-289.905	O_2	-289.905						

4 The tested OER pathway on Ru/Fe_2O_3 (110) in acidic media — In alkaline media pH = 14

4*0.0592pH

	E (DFT) / eV	Δ*G* / eV	G / eV			0 V	1.23 V	Overpotential	0 V	0.401 V	Overpotential
Slab-1	-257.1019347	0	-257.1019347	$+2H_2O$	-285.5419347	0	0	0	0	0	0
OH	-270.493058	0.330535	-270.162523	$+H_2O+1/2\ H_2$	-287.782523	-2.24058833	-3.47059	-3.47059	-3.06959	-3.47059	-3.47058833
O	-262.0556966	0.051366	-262.0043306	$+H_2O+H_2$	-283.0243306	2.517604088	0.057604	3.528192	0.859604	0.057604	**3.528192418**
OOH	-271.8675738	0.374605	-271.4929688	$+3/2\ H_2$	-281.6929688	3.84896588	0.158966	0.101362	1.362966	0.159966	0.102361792
Slab-2	-257.1019347	0	-257.1019347	$+O_2+2H_2$	-280.6119347	4.93	0.01	-0.14897	1.615	0.011	-0.14896588
O_2	-289.963	0.058	-289.905	O_2	-289.905						

5 The tested OER pathway on Ru/Fe_2O_3 (110) in acidic media — In alkaline media pH = 14

									4*0.0592pH		
	E (DFT) / eV	Δ*G* / eV	G / eV			0 V	1.23 V	Overpotential	0 V	0.401 V	Overpotential
Slab-1	-257.1019347	0	-257.1019347	$+2H_2O$	-285.5419347	0	0	0	0	0	0
OH	-268.5715249	0.330535	-268.2409899	$+H_2O+1/2\ H_2$	-285.8609899	-0.31905518	-1.54906	-1.54906	-1.14806	-1.54906	-1.54905518
O	-262.0556966	0.051366	-262.0043306	$+H_2O+H_2$	-283.0243306	2.517604088	0.057604	1.606659	0.859604	0.057604	1.606659268
OOH	-271.8675738	0.374605	-271.4929688	$+3/2\ H_2$	-281.6929688	3.84896588	0.158966	0.101362	1.362966	0.159966	0.102361792
Slab-2	-257.1019347	0	-257.1019347	$+O_2+2H_2$	-280.6119347	4.93	0.01	-0.14897	1.615	0.011	-0.14896588
O_2	-289.963	0.058	-289.905	O_2	-289.905						

6 The tested OER pathway on Ru/Fe_2O_3 (110) in acidic media — In alkaline media pH = 14

									4*0.0592pH		
	E (DFT) / eV	Δ*G* / eV	G / eV			0 V	1.23 V	Overpotential	0 V	0.401 V	Overpotential
Slab-1	-257.1019347	0	-257.1019347	$+2H_2O$	-285.5419347	0	0	0	0	0	0
OH	-267.6947653	0.310396	-267.3843693	$+H_2O+1/2\ H_2$	-285.0043693	0.53756544	-0.69243	-0.69243	-0.29143	-0.69243	-0.69243456
O	-262.3102546	0.020213	-262.2900416	$+H_2O+H_2$	-283.3100416	2.23189314	-0.22811	0.464328	0.573893	-0.22811	0.4643277
OOH	-271.7712825	0.289386	-271.4818965	$+3/2\ H_2$	-281.6818965	3.86003815	0.170038	0.398145	1.374038	0.171038	0.39914501
Slab-2	-257.1019347	0	-257.1019347	$+O_2+2H_2$	-280.6119347	4.93	0.01	-0.16004	1.615	0.011	-0.16003815
O_2	-289.963	0.058	-289.905	O_2	-289.905						

Figure S21. The DFT-testing process for finding optimal active site of alkaline OER on Ru/Fe_2O_3 (110), suggesting site 6 is the optimal active site.

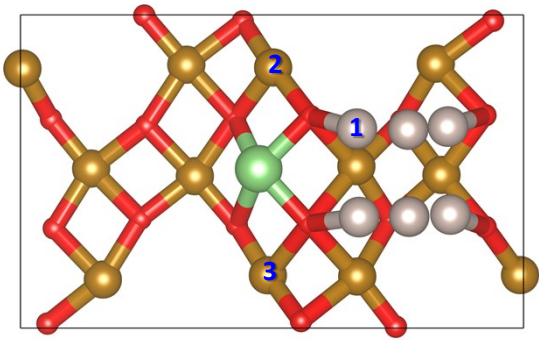

Fe Li Ru O

1	The tested OER pathway on Ru/Fe_2O_3 (110)-Li in acidic media								In alkaline media pH=14		
									4*0.0592pH		
	E (DFT) / eV	Δ*G* / eV	G / eV			0 V	1.23 V	Overpotential	0 V	0.401 V	Overpotential
Slab-1	-262.3546968	0	-262.3546968	$+2H_2O$	-290.7946968	0	0	0	0	0	0
OH	-274.2123743	0.274	-273.9383743	$+H_2O+1/2\ H_2$	-291.5583743	-0.76367745	-1.99368	-1.99368	-1.59268	-1.99368	-1.99367745
O	-270.6847313	0.025	-270.6597313	$+H_2O+H_2$	-291.6797313	-0.88503453	-3.34503	-1.35136	-2.54303	-3.34503	**-1.35135708**
OOH	-277.0082812	0.334	-276.6742812	$+3/2\ H_2$	-286.8742812	3.92041558	0.230416	3.57545	1.434416	0.231416	3.57645011
Slab-2	-262.3546968	0	-262.3546968	$+O_2+2H_2$	-285.8646968	4.93	0.01	-0.22042	1.615	0.011	-0.22041558
O_2	-289.963	0.058	-289.905	O_2	-289.905						

2	The tested OER pathway on Ru/Fe_2O_3 (110)-Li in acidic media								In alkaline media pH=14		
									4*0.0592pH		
	E (DFT) / eV	Δ*G* / eV	G / eV			0 V	1.23 V	Overpotential	0 V	0.401 V	Overpotential
Slab-1	-262.3546968	0	-262.3546968	$+2H_2O$	-290.7946968	0	0	0	0	0	0
OH	-273.0618009	0.274	-272.7878009	$+H_2O+1/2\ H_2$	-290.4078009	0.38689594	-0.8431	-0.8431	-0.4421	-0.8431	-0.84310406
O	-268.0083556	0.025	-267.9833556	$+H_2O+H_2$	-289.0033556	1.79134119	-0.66866	0.174445	0.133341	-0.66866	**0.17444525**
OOH	-277.0082812	0.334	-276.6742812	$+3/2\ H_2$	-286.8742812	3.92041558	0.230416	0.899074	1.434416	0.231416	0.90007439
Slab-2	-262.3546968	0	-262.3546968	$+O_2+2H_2$	-285.8646968	4.93	0.01	-0.22042	1.615	0.011	-0.22041558
O_2	-289.963	0.058	-289.905	O_2	-289.905						

3	The tested OER pathway on Ru/Fe_2O_3 (110)-Li in acidic media								In alkaline media pH=14		
									4*0.0592pH		
	E (DFT) / eV	Δ*G* / eV	G / eV			0 V	1.23 V	Overpotential	0 V	0.401 V	Overpotential
Slab-1	-262.3546968	0	-262.3546968	$+2H_2O$	-290.7946968	0	0	0	0	0	0
OH	-272.4013641	0.330535	-272.0708291	$+H_2O+1/2\ H_2$	-289.6908291	1.1038677	-0.12613	-0.12613	0.274868	-0.12613	-0.1261323
O	-267.7519121	0.051366	-267.7005461	$+H_2O+H_2$	-288.7205461	2.0741507	-0.38585	-0.25972	0.416151	-0.38585	**-0.259717**
OOH	-277.3059275	0.374605	-276.9313225	$+3/2\ H_2$	-287.1313225	3.6633743	-0.02663	0.359224	1.177374	-0.02563	0.3602236
Slab-2	-262.3546968	0	-262.3546968	$+O_2+2H_2$	-285.8646968	4.93	0.01	0.036626	1.615	0.011	0.0366257
O_2	-289.963	0.058	-289.905	O_2	-289.905						

Figure S22. The DFT-testing process for finding optimal active site of alkaline OER on Ru/Fe_2O_3 (110)-Li, suggesting site 3 is the optimal active site.

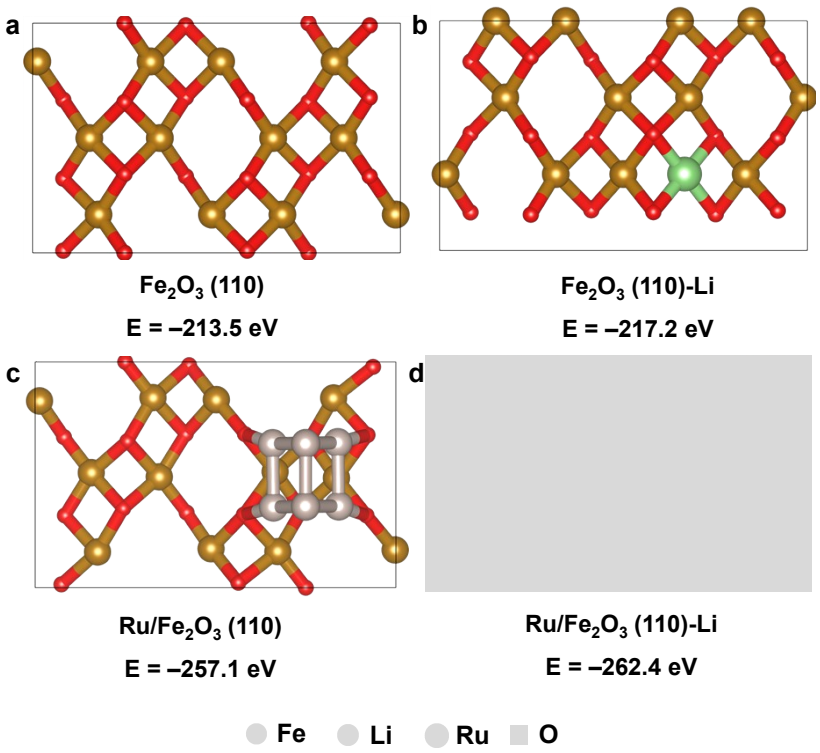

Figure S23. The calculated surface free energy of Fe_2O_3 (110), Fe_2O_3 (110)-Li, Ru/Fe_2O_3 (110), and Ru/Fe_2O_3 (110)-Li catalysts.

Table S1. Comparison for HER activity of Ru/Fe_2O_3-Li with currently reported noble metal-based catalysts in 1.0 M KOH electrolyte.

Catalysts	Overpotential @ 10 mA cm^{-2} (mV)	Tafel slope (mV/dec)	References
Ru/Fe_2O_3-Li	21 mV	39.8	*This work*
Pt_{tet}@$Ni(OH)_2$	—	27	19
Cl-Pt/LDH	25.2	24.3	20
Pt/MgO	39	39	21
PtC_{60}	24.3	41.9	22
Pt_{SA}-NiO/Ni	26	27.07	23
Ru-1.0	13	25.3	24
Ir-NSG	18.5	28.3	25

References

1 Y. Lin, Z. Tian, L. Zhang, J. Ma, Z. Jiang, B. J. Deibert, R. Ge, L. Chen, Chromium-ruthenium oxide solid solution electrocatalyst for highly efficient oxygen evolution reaction in acidic media. *Nat. Commun.* 2019, **10**, 162.

2 H. Su, W. Zhou, W. Zhou, Y. Li, L. Zheng, H. Zhang, M. Liu, X. Zhang, X. Sun, Y. Xu, F. Hu, J. Zhang, T. Hu, Q. Liu, S. Wei, In-situ spectroscopic observation of dynamic-coupling oxygen on atomically dispersed iridium electrocatalyst for acidic water oxidation. *Nat. Commun*. 2021, **12**, 6118.

3 G. Kresse, J. Hafner, Ab initio molecular dynamics for liquid metals. *Phys. Rev. B.* 1993, **47**, 558.

4 G. Kresse, J. Furthmüller, Efficiency of ab-initio total energy calculations for metals and semiconductors using a plane-wave basis set. *Comput. Mater. Sci.* 1996, **6**, 15-50.

5 P. E. Blöchl, Projector augmented-wave method. *Phys. Rev. B.* 1994, **50**, 17953.

6 G. Kresse, D. Joubert, From ultrasoft pseudopotentials to the projector augmented-wave method. *Phys. Rev. B.* 1999, **59**, 1758.

7 J. P. Perdew, K. Burke, M. Ernzerhof, Generalized gradient approximation made simple. *Phys. Rev. Lett*. 1996, **77**, 3865.

8 G. Kresse, J. Furthmüller, Efficient iterative schemes for ab-initio total energy calculations using a plane wave basis set. *Phys. Rev. B.* 1996, **54**, 11169.

9 H. J. Monkhorst, J. D. Pack, Special points for Brillouin-zone integrations. *Phys. Rev. B.* 1976, **13**, 5188.

10 X. Li, Z. Wang, Z. Su, Z. Zhao, Q. Cai, J. Zhao, Phthalocyanine-supported single-atom catalysts as a promising bifunctional electrocatalyst for ORR/OER: A computational study. *ChemPhysMater* 2022, **1**, 237-245.

11 S. Grimme, Semiempirical GGA-type density functional constructed with a long-range dispersion correction. *J. Comput. Chem*. 2006, **27**, 1787-1799.

12 K. Mathew, R. Sundararaman, K. Letchworth-Weaver, T. A. Arias, R. G. Hennig, Implicit solvation model for density-functional study of nanocrystal surfaces and

reaction pathways. *J. Chem. Phys*. 2014, **140**, 084106.

13 G. Henkelman, A. Arnaldsson, H. Jónsson, A fast and robust algorithm for Bader decomposition of charge density. *Comput. Mater. Sci*. 2006, **36**, 354-360.

14 R. F. W. Bader, A quantum theory of molecular structure and its applications. *Chem. Rev.* 1991, **91**, 893-928.

15 J. K. Nørskov, T. Bligaard, A. Logadottir, Trends in the exchange current for hydrogen evolution. *J. Electrochem. Soc.* 2005, **152**, J23.

16 M. del Cueto, P. Ocón, J. M. L. Poyato, Comparative study of oxygen reduction reaction mechanism on nitrogen-, phosphorus-, and boron-doped graphene surfaces for fuel cell applications. *J. Phys. Chem. C* 2015, **119**, 2004-2009.

17 J. K. Nørskov, J. Rossmeisl, A. Logadottir, L. Lindqvist, J. R. Kitchin, T. Bligaard, H. Jónsson, Origin of the overpotential for oxygen reduction at a fuel-cell cathode. *J. Phys. Chem. B* 2004, **108**, 17886-17892.

18 H. Ma, X. Zhou, J. Li, H. Cheng, J. Ma, Rational design of heterostructured nanomaterials for accelerating electrocatalytic hydrogen evolution reaction kinetics in alkaline media. *J. Electrochem*. 2024, **30**, 2305101.

19 C. Wan, Z. Zhang, J. Dong, M. Xu, H. Pu, D. Baumann, Z. Lin, S. Wang, J. Huang, A. H. Shah, X. Pan, T. Hu, A. N. Alexandrova, Y. Huang, X. Duan, Amorphous nickel hydroxide shell tailors local chemical environment on platinum surface for alkaline hydrogen evolution reaction. *Nat. Mater.* 2023, **22**, 1022-1029.

20 T. Zhang, J. Jin, J. Chen, Y. Fang, X. Han, J. Chen, Y. Li, Y. Wang, J. Liu, L. Wang, Pinpointing the axial ligand effect on platinum single-atom-catalyst towards efficient alkaline hydrogen evolution reaction. *Nat. Commun.* 2022, **13**, 6875.

21 H. Tan, B. Tang, Y. Lu, Q. Ji, L. Lv, H. Duan, N. Li, Y. Wang, S. Feng, Z. Li, C. Wang, F. Hu, Z. Sun, W. Yan, Engineering a local acid-like environment in alkaline medium for efficient hydrogen evolution reaction. *Nat. Commun*. 2022, **13**, 2024.

22 J. Chen, M. Aliasgar, F. B. Zamudio, T. Zhang, Y. Zhao, X. Lian, L. Wen, H. Yang, W. Sun, S. M. Kozlov, W. Chen, L. Wang, Diversity of platinum-sites at

platinum/fullerene interface accelerates alkaline hydrogen evolution. *Nat. Commun*. 2023, **14**, 1711.

23 K. L. Zhou, Z. Wang, C. B. Han, X. Ke, C. Wang, Y. Jin, Q. Zhang, J. Liu, H. Wang, H. Yan, Platinum single-atom catalyst coupled with transition metal/metal oxide heterostructure for accelerating alkaline hydrogen evolution reaction. *Nat. Commun*. 2021, **12**, 3783.

24 Q. Hu, K. Gao, X. Wang, H. Zheng, J. Cao, L. Mi, Q. Huo, H. Yang, J. Liu, C. He, Subnanometric Ru clusters with upshifted d band center improve performance for alkaline hydrogen evolution reaction. *Nat. Commun.* 2022, **13**, 3958.

25 Q. Wang, C. Xu, W. Liu, S. Hung, H. B. Yang, J. Gao, W. Cai, H. M. Chen, J. Li, B. Liu, Coordination engineering of iridium nanocluster bifunctional electrocatalyst for highly efficient and pH-universal overall water splitting. *Nat. Commun.* 2020, **11**, 4264.